Enhancement of Cell Adhesion on 3D-Printed PLA through Surface Modification Using Photo-Activated Chlorine Dioxide

Nana Otsuka[1], Yasuo Yagura[1], Tsuyoshi Inoue[1,2], Tetsushi Taguchi[3], Akihiro Nishiguchi[3], Haruyasu Asahara*[1,2]

[1] Graduate School of Pharmaceutical Sciences, The University of Osaka, Yamadaoka 1-6, Suita, Osaka, 565-0871, Japan.

[2] Institute for Open and Transdisciplinary Research Initiatives, The University of Osaka, Yamadaoka 1-6, Suita, Osaka, 565-0871, Japan.

[3] Research Center for Macromolecules and Biomaterials, National Institute for Materials Science, Namiki 1-1, Tsukuba, Ibaraki, 305-0044, Japan.

* Email: asahara@phs.osaka-u.ac.jp

Keywords: Polylactic acid (PLA), Photo-oxidation, Carboxy functionalization, Surface charge density, Cell adhesion, 3D-printed scaffolds

Abstract

Poly(lactic acid) (PLA) has attracted considerable attention as a scaffold material in tissue engineering because of its biocompatibility, biodegradability, and suitable mechanical strength. However, PLA's inherent hydrophobicity limits its cell affinity. To address this limitation, several surface modification strategies have been developed; nevertheless, challenges remain, including reduced mechanical strength, limited applicability to three-dimensional structures, and procedural complexity. In response, a surface modification method, termed "photo-oxidation," was developed. This method utilizes reactive species generated by light irradiation of chlorine dioxide radicals and overcomes the aforementioned challenges. In this study, PLA was oxidized using the photo-oxidation method, and its cell affinity was evaluated using mouse fibroblasts (L929 cells). The results showed that photo-oxidation at an appropriate temperature significantly enhanced cell affinity, as evidenced by increased cell numbers and pronounced actin extension. Furthermore, this method was successfully applied to three-dimensional structures, demonstrating its potential as a versatile strategy for improving the biological performance of PLA.

1. Introduction

Polylactic acid (PLA) is widely recognized as a polymeric material that combines excellent biocompatibility, biodegradability, and mechanical strength. These attributes have made PLA a subject of extensive research for its potential use as a scaffold material in tissue engineering.[1–3] Scaffolds are a fundamental component of regenerative medicine, working in conjunction with cells and growth factors to facilitate tissue repair and regeneration.[4] Their primary role is to enable the formation of complex three-dimensional (3D) structures, such as organs, by providing a framework that maintains the desired tissue architecture and actively influences cellular differentiation. Ideally, scaffolds should possess sufficient mechanical strength to withstand forces encountered during tissue formation and should degrade and be resorbed by the body once structural support is no longer required. Despite its favorable properties, PLA has a major drawback—its inherent hydrophobicity. On hydrophobic surfaces, cell-adhesive proteins such as fibronectin are prone to denaturation upon adsorption, which compromises cell–protein interactions and reduces cell compatibility.[5] In addition, inflammatory responses can be triggered in surrounding tissues in contact with the material, and the acidic nature of PLA degradation products may exacerbate resorption at the implantation site.[6]

Therefore, several investigations have been reported that modify the materials used in the fabrication of 3D structures to improve their hydrophilicity.[7] These strategies include synthesizing copolymers of PLA with other monomers and creating composite materials by incorporating PLA with other substances.[8–10] However, modifying and functionalizing the surfaces of molded (3D) structures remains a challenge.[11,12]

Surface modification makes it possible to control a material's surface properties without altering its bulk properties. Conventional approaches for surface modification of polymeric materials

include chemical treatments[13] such as those employing bases or strong acids; physical treatments[14] such as plasma treatment or corona discharge; and polymer reactions[15] such as graft polymerization. Although various surface modification methods have been developed, they still present difficulties. For example, plasma treatment is simple and widely used; however, because the modification predominantly occurs on surfaces directly exposed to the plasma, uniform treatment of complex 3D structures or internal regions of porous materials is limited. Moreover, hydrophobic recovery over time remains a concern. Similarly, alkaline hydrolysis is an effective approach for introducing carboxy groups onto polyester-based materials, but it involves cleavage of ester bonds, which can lead to surface erosion, decreased molecular weight, and deterioration of mechanical properties. Consequently, there is an urgent need to develop novel modification methods that can be applied to 3D structures with complex scaffold geometries.

In this context, we have developed a surface modification method using chlorine dioxide radicals ($ClO_2^{\bullet}$) under photoirradiation (photo-oxidation). This photochemical reaction generates active species that oxidize even stable and strong C–H bonds.[16] We have previously demonstrated the introduction of oxygen-containing functional groups into polymer resins such as polypropylene (PP), which possesses inert C–H bonds, under mild conditions of room temperature and atmospheric pressure.[17] Furthermore, we have shown that $ClO_2^{\bullet}$ photo-oxidation can be applied to the internal oxidation of complex 3D structures through oxidative functionalization of PP nonwoven fabrics[18] It has also been demonstrated that carboxy groups can be introduced onto the PLA surface by applying $ClO_2^{\bullet}$ photo-oxidation.[19] Unlike plasma or alkaline hydrolysis, the photo-oxidation method employed in this study proceeds via gas-phase oxidizing species activated by light, without requiring direct irradiation of the substrate. Consequently, the reaction can occur in regions accessible to the oxidizing species, including concave surfaces and internal spaces of 3D

structures. In addition, because the reaction does not involve bulk hydrolysis, surface functionalization can be achieved while maintaining the structural integrity of the substrate. Therefore, this method offers practical advantages over conventional approaches in terms of applicability to 3D structures and suppression of substrate degradation.

In this study, we investigated the enhancement of the cell affinity of PLA materials through photo-oxidation. In particular, we focused on the surface modification and cell attachment of molded structures fabricated using a 3D printer. Specifically, we applied photo-oxidation to both PLA films and 3D-printed structures and evaluated the surface properties of the modified PLA, including the number of introduced functional groups and the surface morphology. Subsequently, we cultured mouse fibroblast cells (L929) on the modified PLA films and assessed cell affinity based on cell number and morphology. The photo-oxidation method was also applied to 3D-printed scaffolds, where we confirmed that surface modification was uniformly achieved throughout the entire structure. Furthermore, we evaluated the cell affinity of the oxidized 3D scaffolds.

2. Experimental Section

2.1.Materials

PLA pellets (Luminy L105) were purchased from Total Corbion. PLA filament for the 3D printer was obtained from Beijing Tiertime Technology Co. (Beijing, China). Sodium chlorite ($NaClO_2$) and fetal bovine serum were purchased from Sigma–Aldrich (St. Louis, MO, USA). Hydrochloric acid (HCl, 35.0–37.0%), ethanol (99.5%), 1 mol/L sodium hydroxide (NaOH), RPMI-1640 medium, 4% paraformaldehyde phosphate buffer solution (PFA), bovine serum albumin, Triton X-100, and 4′,6-diamidino-2-phenylindole (DAPI) were purchased from FUJIFILM Wako Pure

Chemical Co. (Tokyo, Japan). Toluidine blue O (TBO), sodium dodecyl sulfate (SDS), Cell Count Reagent SF (WST-8), and Dulbecco's phosphate-buffered saline (PBS) were purchased from Nacalai Tesque (Kyoto, Japan). Dimethylamine (DA), 1-(3-dimethylaminopropyl)-3-ethylcarbodiimide hydrochloride (EDC·HCl), trifluoroacetic anhydride (TFAA), *N*,N′-di-*tert*-butylcarbodiimide (DBC), and 2,2,2-trifluoroethanol (TFE) were purchased from Tokyo Chemical Industry (Tokyo, Japan). Pyridine was purchased from Kishida Chemical Co., Ltd. (Osaka, Japan). Penicillin–streptomycin (10,000 U/mL), TrypLE Express Enzyme (1×), phenol red, and rhodamine phalloidin were purchased from Thermo Fisher Scientific K.K. (Tokyo, Japan). L929 mouse fibroblast cells (EC85011425) were obtained from KAC Co. (Kyoto, Japan).

2.2.PLA Sample Preparation

–Films

PLA pellets (2.7 g) were placed in a 200-μm-thick mold and melted at 175 °C for 3 minutes. The molten PLA was then heat-pressed at 175 °C and 10 MPa for 3 minutes.

–3D structures

A desktop 3D printer (UP Plus2, Beijing Tiertime Technology Co., Ltd., China) was used to fabricate hollow quadrangular column samples with a width of 10 mm, depth of 9 mm, height of 5 mm, and wall thickness of 1 mm. The printing density was set to 15%.

2.3.Oxidation of PLA using photoactivated $ClO_2^{\bullet}$

PLA samples were photo-oxidized under irradiation with a 60-W LED lamp (λ = 365 nm, 5 mW/cm^2) using $ClO_2^{\bullet}$ generated from an aqueous solution (20 mL) of $NaClO_2$ (200 mg) and 35% HCl (100 μL). Oxidation was performed using the glassware system reported previously.[17,18,20] $ClO_2^{\bullet}$ solution was added to the outer groove of the glassware, and the sample was placed inside.

During the reaction, the samples were shielded from direct UV irradiation using aluminum sheets. Reactions were conducted at 30, 60, and 80 °C for 30 minutes. For PLA films, oxidation was performed for 15 minutes on each side, and the $ClO_2^{\bullet}$ solution was replaced every 15 minutes. After oxidation, the samples were washed with distilled water and air-dried. The photo-oxidized samples were designated Ox-30, Ox-60, and Ox-80.

2.4.Plasma treatment of PLA samples

Plasma treatment was performed using a tabletop vacuum plasma system (YHS-R, SAKIGAKE-Semiconductor Co., Ltd., Japan). PLA film samples were placed on a sample tray, and vacuum was generated using a vacuum pump. After the desired vacuum pressure was reached, a plasma discharge was applied for 1 minute. The samples were then washed with distilled water and air-dried. Plasma-treated samples were designated as Plasma.

2.5.Amidation of photo-oxidized PLA

Ox-30 and Ox-60 samples were subjected to amidation with DA as follows. Samples were immersed in 10 mL of an aqueous solution containing 2 mM EDC·HCl and 2 mM DA at room temperature for 18 hours. The samples were then washed three times with distilled water and air-dried. The resulting samples were designated as Ox-30-DA and Ox-60-DA, respectively. For comparison, amidation was also performed using an EDC/NHS activation system under otherwise identical conditions.

2.6.Alkaline hydrolysis treatment of PLA

Alkaline hydrolysis-treated samples were prepared as a conventional comparison as follows. PLA films were immersed in 2 M NaOH aqueous solution (prepared by diluting an 8 M NaOH solution fourfold with Milli-Q water) at room temperature for 3 h. The treatment time was determined based on preliminary water contact angle measurements to achieve a wettability level comparable to that of the photo-oxidized samples, enabling a fair comparison. After treatment, the samples were thoroughly washed with Milli-Q water and dried under reduced pressure overnight. The resulting samples are referred to as Alkali-treated PLA in this study.

2.7.Quantitative analysis of functional groups using gas-phase chemical processing and X-ray photoelectron spectroscopy (XPS)

Oxygen-containing functional groups on the PLA surface were modified with fluorine-containing functional groups by reacting hydroxy groups with anhydrous TFAA and carboxy groups with TFE in the gas phase. Following these modifications, XPS was performed to quantify the degree of functionalization. The percentages of carbon (C) and fluorine (F) atoms were obtained from XPS data, and the proportion of functionalized carbon atoms relative to the total carbon content was calculated using Eq. (1):

$$\text{Percentage of functionalized carbon atoms (\%)} = \frac{\frac{1}{3}[F]}{[C] - \frac{2}{3}[F]} \quad (1)$$

where [F] is the atomic percentage (at%) of fluorine and [C] is the at% of carbon. XPS measurements were conducted using a KRATOS ULTRA2 system (Shimadzu Corporation, Japan) equipped with a monochromatic Al Kα source (1486.6 eV) operating at 225 W.

–Modification of hydroxy groups with TFAA

The reaction was conducted in the gas phase to avoid direct contact between the sample and the reagent. PLA film samples were placed upright in a microtube, and 2 mL of TFAA was added to

a screw-cap tube containing the microtube. The tube was sealed and maintained at 30 °C for 18 h to allow the reaction to proceed.

–Modification of carboxy groups with TFE

Similarly, carboxy groups were modified in the gas phase to prevent direct contact between the sample and the reagents. PLA film samples were placed upright in a microtube along with 0.3 mL DBC, 0.9 mL TFA, and 0.4 mL pyridine in a screw-cap tube. The tube was sealed and maintained at 30 °C for 18 h to complete the reaction.

2.8.Zeta potential measurement

The zeta potential of PLA films was measured using a Zeta Potential, Particle Size, and Molecular Weight Measurement System (ELSZ-2000ZS, Otsuka Electronics Co., Japan). The surface zeta potential was determined using the flat-cell unit of the instrument, with two drops of the particle suspension added to 10 mM NaCl solution.

2.9.Quantification of carboxy groups on the PLA surface

The carboxy groups on the PLA surface were quantified using the TBO assay according to a previously reported method.[21] PLA samples were incubated in 4 mL of TBO solution (0.1% TBO in 1 mM NaOH) at 40 °C for 30 minutes and then washed with 1 mM NaOH. This washing process was repeated until the supernatant became clear. TBO was then desorbed by incubating the samples in 4 mL of 20% SDS solution. The TBO concentration in the SDS supernatant was determined by measuring absorbance at 630 nm using a UV–visible (UV–Vis) spectrophotometer (V-750, Jasco Corporation, Japan). The surface carboxy group concentration per unit mass of PLA

(mol/g) was calculated using Eq. (2), assuming that TBO binds stoichiometrically (1:1) to negatively charged carboxy groups:

$$\text{Surface carboxy group concentration (mol/g)} = \frac{C_{TBO} \times V_{SDS}}{M_{PLA}} \quad (2)$$

where C_{TBO} is the concentration of TBO in the SDS supernatant (mol/L), V_{SDS} is the volume of the SDS solution (L), and M_{PLA} is the mass of the PLA sample (g). Results represent the mean of three independent measurements.

2.10. Surface analysis

–Water Contact Angle Measurement

Static contact angles were measured using a contact angle meter (DMo-501, Kyowa Interface Science Co., Japan). Approximately 1-μL droplets of distilled water were dispensed onto the PLA substrates, and the static contact angles were determined from still frames using the sessile drop approximation. Results represent the mean of five independent measurements.

–Fourier Transform Infrared (FT-IR) Spectroscopy

Functional groups were identified at room temperature by FT-IR spectroscopy using a Spectrum TWO spectrometer (PerkinElmer, USA) equipped with a diamond window.

–Observation of surface morphology by SEM

The surface morphology of PLA samples was examined using a Schottky field-emission scanning electron microscope (JSM-F100, JEOL Ltd., Japan). Sample surfaces were coated with osmium to a thickness of approximately 5 nm, and imaging was performed at an accelerating voltage of 3–5 kV.

2.11.Cell Culture

L929 mouse fibroblast cells were cultured in RPMI-1640 medium supplemented with 10% fetal bovine serum and 1% penicillin–streptomycin in a humidified incubator maintained at 37 °C with 5% CO_2. Cells were detached with TrypLE Express Enzyme every 3–4 days, and passaging was performed. Cells at passages 10–30 were used in the experiments.

2.12.Cell adhesion

–Seeding of cells onto PLA films

PLA films were cut into circles 9 mm in diameter and photo-oxidized. PLA film samples and cloning rings were sequentially placed in 48-well plates and sterilized by immersion in 70% ethanol for 5 minutes. The samples were then washed with PBS. A 500-μL suspension of L929 cells (1.0×10^4–3.0×10^5 cells/well) was seeded onto the PLA films and incubated for 3 or 4 days at 37 °C in a humidified incubator with 5% CO_2.

–Seeding of Cells onto 3D-Structured PLA

After photo-oxidation, 3D-structured PLA samples were placed in 24-well plates and sterilized with 70% ethanol. The samples were washed with PBS, immersed in 1 mL of cell suspension, and incubated. A 1-mL suspension of L929 cells (1.0×10^4 cells/well) was seeded onto the 3D structures and incubated for 3 days at 37 °C in 5% CO_2.

2.13.Cell count assay

Cell proliferation activity was assessed using the WST-8 assay. After the specified incubation period, samples were washed with PBS to remove unattached cells. Culture medium and WST-8 solution (10% of the medium volume) were added and incubated in a CO_2 incubator for 3 hours. After incubation, the supernatant was transferred to a fresh plate, and absorbance at 450 nm was

measured with a microplate reader (SpectraMax MS, Molecular Devices, Japan). Cell numbers were calculated from a previously prepared calibration curve.

2.14.Observation of cell morphology

Cells were incubated for the specified period and washed with PBS to remove nonadherent cells. The adherent cells were fixed with 4% PFA and subsequently stained with DAPI and rhodamine phalloidin. Stained cells were observed using a confocal microscope (BZ-X800, Keyence, Japan).

Rhodamine phalloidin–stained actin images were used to evaluate cell morphology. Image thresholding was applied to generate binary images, and ImageJ software was used to measure cell area and circularity.

2.15.Tensile test

Tensile tests were performed using a universal testing machine (EZ-S, Shimadzu Co., Japan) with a 500 N load cell at a strain rate of 1 mm/min. Three samples from each group were analyzed, and the average value ± standard deviation is reported.

3. Results and Discussion

3.1.Surface characterization of photo-oxidized PLA

3.1.1.Evaluation of functional groups on the PLA surface

Previous studies have reported that photo-oxidation of PLA introduces carboxy groups.[19] To quantify the amount of carboxy groups introduced under the processing conditions used in this study, a TBO assay was performed (Table 1). The results showed that the number of carboxy groups increased following photo-oxidation. Furthermore, photo-oxidation at 60 °C resulted in

approximately a 17-fold increase in carboxy groups compared with treatment at 30 °C. In addition, XPS elemental analysis based on the previously reported gas-phase chemical modification method was applied to determine the types of oxygen-containing functional groups introduced.[22] As shown in Table 2, the amount of carboxy groups increased as a result of photo-oxidation treatment, with a greater increase observed at 60 °C than at 30 °C. In contrast, the amount of hydroxy groups in both Ox-30 and Ox-60 samples remained nearly the same as in the pristine PLA. Taken together, these results indicate that carboxy groups were preferentially introduced regardless of the photo-oxidation temperature. Notably, a significant difference was observed between the increase in carboxy groups measured by chemical-modification XPS and the TBO assay. This discrepancy is likely attributable to the difference in analysis depth between the two methods: XPS probes only a few nanometers from the material surface, whereas the TBO assay can detect carboxy groups located deeper within the sample.

Table 1. Quantification of surface carboxy (–COOH) groups on PLA samples. Data are expressed as mean ± standard deviation (n = 3).

Sample	Surface –COOH Groups (μmol/g)
Pristine	0.0076 ± 0.0045
Ox-30	0.10 ± 0.031
Ox-60	1.7 ± 0.30

Table 2. Relative abundance of surface functional groups (COOH and OH) on PLA film samples as determined by XPS analysis. Values represent the percentage of each functional group relative to total carbon.

Sample	COOH (%)	OH (%)
Pristine	0.24	0.35
Ox-30	1.08	0.32
Ox-60	1.90	0.35

3.1.2. Surface morphological analysis of photo-oxidized PLA and its derivatives

Surface zeta potential, hydrophilicity (evaluated by water contact angle, WCA), and surface morphology were analyzed for the samples. These evaluations were performed after photo-oxidation and subsequent immersion in ethanol for sterilization prior to cell seeding. The WCA serves as an indicator of hydrophilicity, and previous studies have reported that cells adhere most efficiently to substrates with a WCA of approximately 70°.[23] Furthermore, the degree of oxidation can be controlled by adjusting the oxidation conditions,[19] with temperature being a particularly influential factor. It has been reported that hydrophilicity can be markedly improved by increasing the reaction temperature above the glass transition temperature of PLA. Table 3 summarizes the amount of carboxy groups, zeta potential, and WCA for the pristine PLA, Ox-30, and Ox-60 samples. Surface morphology as observed by SEM is presented in Figure 1. Although the number of carboxy groups introduced in Ox-30 was relatively low, the surface zeta potential was lower than that of pristine PLA, and the WCA also decreased.

Furthermore, SEM observations revealed the formation of numerous micro-scale surface undulations on Ox-60 PLA. Such micro-scale roughness can reduce the effective solid–liquid

contact area and promote partial air entrapment at the interface, potentially leading to Cassie–Baxter-type wetting behavior.[24,25] Under these conditions, the apparent contact angle may increase despite the presence of hydrophilic functional groups.

Therefore, the high contact angle observed for Ox-60 cannot be explained solely by classical Wenzel-type roughness amplification of an intrinsically hydrophilic surface. Rather, the combined effects of surface chemical heterogeneity and micro-scale roughness likely alter the wetting regime, resulting in an increased apparent contact angle.

While SEM provides qualitative morphological comparison, quantitative nanoscale roughness analysis was not performed in the present study.

Table 3. Surface properties of PLA films (pristine and photo-oxidized). Carboxy groups were quantified by TBO assay (see Table 1), zeta potential was measured in 10 mM NaCl solution (n = 3), and water contact angle (WCA) was determined using the sessile drop method (n = 5). Data are expressed as mean ± standard deviation.

Sample	Zeta Potential (mV)	WCA (°)
Pristine	−22.15 ± 0.47	78.2 ± 0.5
Ox-30	−26.52 ± 1.39	64.5 ± 5.2
Ox-60	−37.02 ± 1.46	97.1 ± 0.5

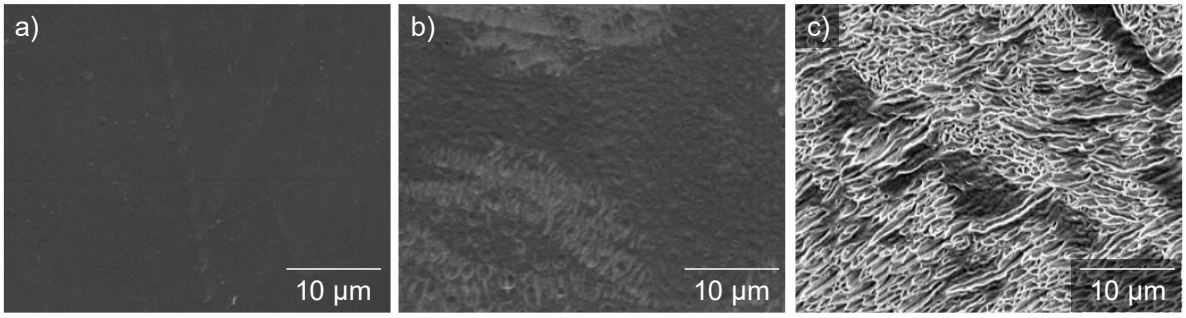

Figure 1. SEM images of PLA films: (a) pristine, (b) Ox-30, and (c) Ox-60.

Comparative experiments revealed no significant difference in the residual surface carboxy group density between the EDC-only and EDC/NHS systems, as determined by the TBO assay (Figure S1). These results indicate that EDC alone is sufficient for effective deactivation of surface carboxy groups under the present conditions. In this carbodiimide-mediated reaction, amide bond formation proceeds via an *O*-acylisourea intermediate, generating an EDC-derived urea by-product, as illustrated schematically in Figure 2a. In the FT-IR spectra, an amide-derived peak appeared around 1600 cm^{-1} for Ox-30-DA but was absent in the pristine and Ox-30 samples (Figure 2b). Furthermore, the TBO assay revealed that the number of carboxy groups in Ox-30-DA was lower than that in Ox-30 (Figure 2c), supporting the conversion of carboxy groups to amides. These results indicate that DA successfully reacted with the carboxy groups, forming amide linkages as

expected. In addition, SEM observations confirmed that DA modification did not cause any significant changes to the surface morphology (Figure 2d).

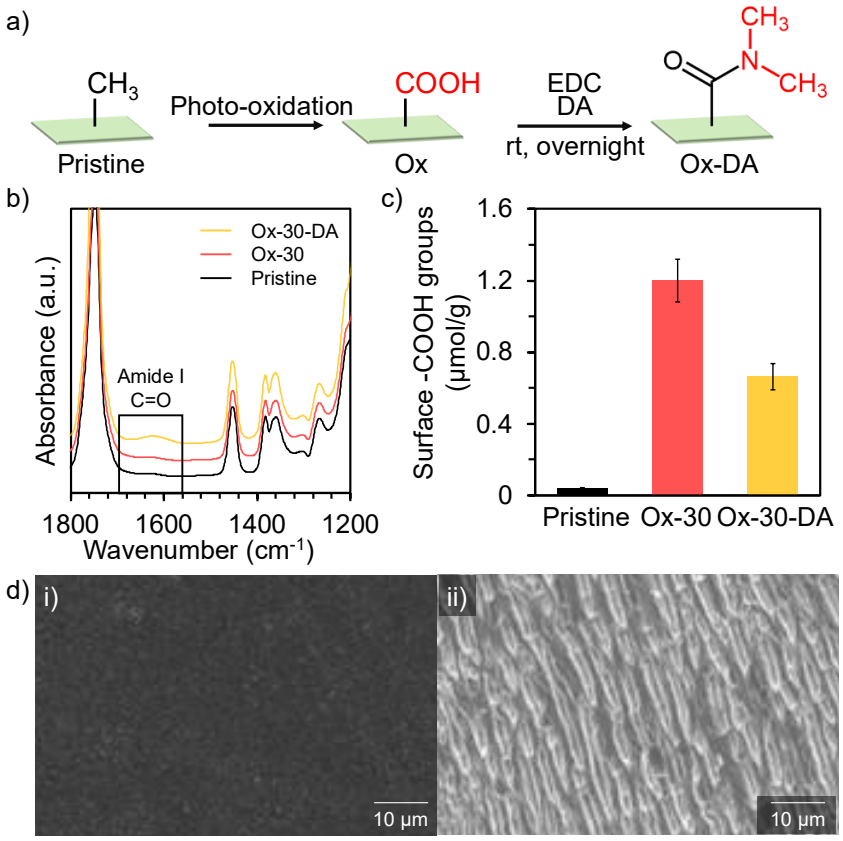

Figure 2. (a) Schematic diagram of amidation. (b) FT-IR spectra of PLA film samples: pristine (black), Ox-30 (red), and Ox-30-DA (blue). (c) Quantification of surface –COOH groups by TBO assay (n = 3). Error bars represent standard deviation. (d) SEM images of PLA films: (i) Ox-30-DA and (ii) Ox-60-DA.

3.1.3.Photo-oxidation of 3D structures

To evaluate the applicability of the photo-oxidation method to 3D structures, photo-oxidation was applied to 3D-printed PLA scaffolds, and the introduction of carboxy groups throughout the

structure was confirmed using the TBO assay. The 3D structures used in this study are shown in Figure 3a. The results of TBO staining for pristine and Ox-30 samples are presented in Figure 3b, where the green region represents the outer surface and the orange region represents the interior. In Ox-30, both the outer and inner regions were stained blue, indicating that the entire 3D structure was successfully modified and carboxy groups were introduced. Next, the oxidation conditions of the 3D structures were optimized (Figure 3c). First, the photo-oxidation time was fixed at 30 minutes, and the treatment was performed at three different temperatures: 30 °C, 60 °C, and 80 °C. Among these, Ox-60 exhibited the highest number of carboxy groups. Subsequently, the treatment temperature was fixed at 60 °C, and the reaction time was varied from 1 to 60 minutes. The sample photo-oxidized for 45 minutes exhibited the highest number of carboxy groups. These results indicate that the number of introduced carboxy groups can be controlled by selecting appropriate treatment temperatures and times. The surface morphology of pristine, Ox-30, and Ox-60 3D structures was examined by SEM (Figure 3d). As with the PLA films, Ox-30 showed no significant morphological changes compared with pristine PLA, whereas Ox-60 displayed noticeable surface roughening. While SEM provides qualitative evidence of surface roughening after oxidation, quantitative roughness analysis of the 3D-printed structures was technically challenging. The as-printed PLA scaffolds inherently possess microscale surface texturing arising from the layer-by-layer fabrication process, which introduces baseline heterogeneity. This intrinsic roughness complicates direct quantitative comparison of treatment-induced roughness changes using localized AFM measurements. Therefore, systematic quantitative roughness evaluation of complex 3D geometries remains a subject for future investigation. Although TBO staining indicates functionalization of both outer and inner scaffold surfaces, region-specific quantification of functional group density was not feasible. Previous studies using the same photo-oxidation

system on polypropylene nonwoven fabrics confirmed internal functionalization by TBO staining,[18] suggesting that oxidation is not strictly limited to the outermost surface. Nevertheless, oxidation uniformity in three-dimensional constructs is expected to depend on scaffold thickness, porosity, oxygen diffusion, and light accessibility. Therefore, while effective modification was observed within the scaffold dimensions employed in this study, systematic evaluation of penetration depth in thicker or more complex geometries will be required to fully assess scalability.

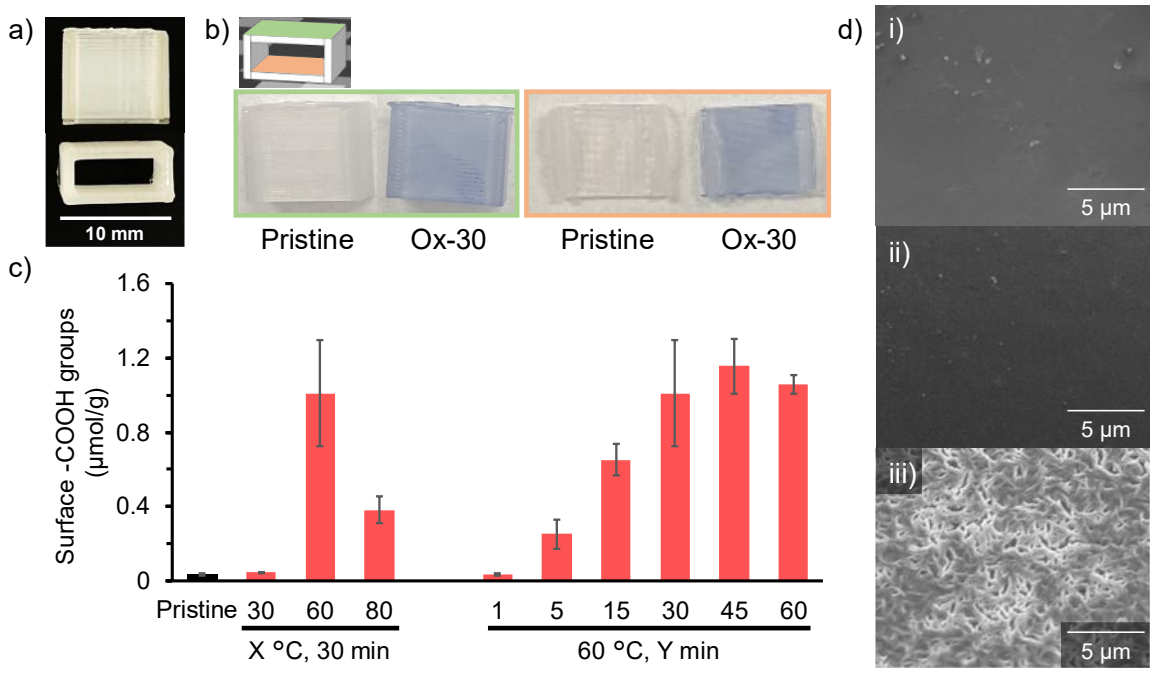

Figure 3. (a) Photograph of a 3D-printed PLA construct (10 mm × 9 mm × 5 mm). (b) TBO-stained images of 3D structures. The green frame highlights the outer region, and the orange frame highlights the interior. (c) Quantification of surface carboxy (–COOH) groups introduced on 3D structures (n = 3). Error bars represent standard deviation. (d) SEM images of 3D structures: (i) pristine, (ii) Ox-30, and (iii) Ox-60.

3.2. Effect of surface modification of PLA on cell adhesion

3.2.1. Protein adsorption behavior

Because initial cell adhesion is mediated by serum protein adsorption, we first evaluated protein adsorption behavior on photo-oxidized surfaces. BSA adsorption assays revealed that Ox-60 exhibited the highest total protein adsorption, followed by Ox-30 and pristine surfaces (Figure 4). Thus, protein adsorption increased with increasing carboxy group density introduced by photo-oxidation.

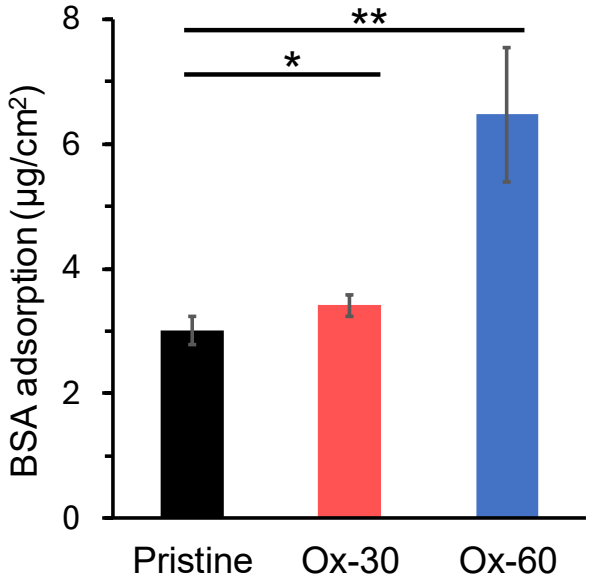

Figure 4. BSA Adsorption on PLA films (n = 4). Statistical significance was determined using the Student's *t*-test. Error bars represent standard deviation. *$p < 0.05$, **$p < 0.01$.

3.2.2 Cell adhesion on films

L929 cells were seeded at a density of 3×10^4 cells/well on PLA films cut into 9-mm-diameter circles and cultured for 4 days. Cell counting was undertaken, and cell morphology was examined (Figure 5a). Fluorescence immunostaining revealed that cells on pristine samples were nearly spherical, whereas those on Ox-30 samples displayed elongated actin filaments and a more spread morphology (Figure 5b). Quantification of cell numbers demonstrated a significant increase on

Ox-30 samples, with approximately 3.0×10^5 cells compared with approximately 1.7×10^5 cells on pristine samples (Figure 5c). Furthermore, analysis of fluorescence-stained images allowed quantification of average cell area and circularity (Figures 5d and 5e). The average cell area on Ox-30 was approximately 1.4-fold higher than on pristine PLA, while circularity was significantly reduced, indicating greater cell spreading. Enhanced cell spreading is commonly associated with integrin-mediated adhesion and focal adhesion maturation, which regulate cytoskeletal organization and cell morphology.[26] Moderately hydrophilic surfaces have been reported to promote favorable protein conformation and integrin engagement, thereby facilitating cell spreading.[27] These findings suggest that photo-oxidation enhanced the cell affinity of PLA films.

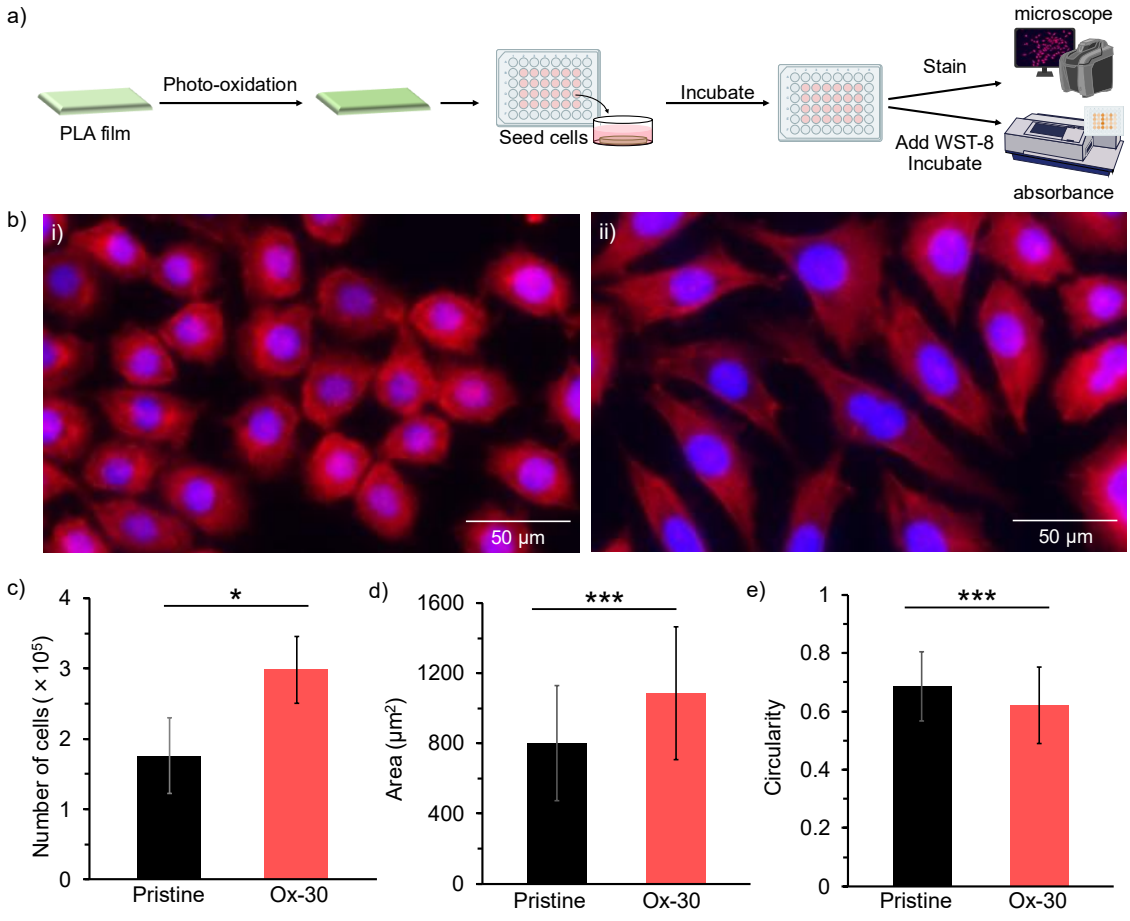

Figure 5. (a) Schematic diagram of the cell seeding and culture experiment. (b) Fluorescence microscopy images of L929 cells stained for actin filaments (red) and nuclei (blue): (i) pristine and (ii) Ox-30. (c) Quantification of adherent cells on PLA films after 4 days of culture (n = 4). Statistical significance was determined using the Student's *t*-test. Error bars represent standard deviation. *$p < 0.05$. (d) Quantification of average cell area and (e) circularity based on fluorescence images using ImageJ (n = 200). Statistical analysis was performed using the Student's *t*-test. Error bars represent standard deviation. *** $p < 0.001$.

Given that photo-oxidation enhanced the cell affinity of PLA films, we further investigated the early-stage adhesion process. L929 cells were seeded at a density of 5×10^5 cells/well on PLA films and cultured for 15–180 minutes. After incubation, adherent cells were quantified and their morphology was assessed. Morphological observations revealed that after 30 minutes of incubation, no cells were detected on pristine PLA, whereas a small number of cells were visible on Ox-30 (Figure 6a). For both pristine and Ox-30 films, the number of adherent cells increased with longer incubation times. Notably, a large number of cells with elongated actin filaments were observed on Ox-30 after 120 minutes of incubation. Quantitative analysis confirmed that Ox-30 significantly increased the number of adherent cells compared with pristine PLA at incubation times ranging from 30 to 180 minutes (Figure 6b). These results suggest that photo-oxidation promotes cell adhesion at the early stages of culture, which may in turn contribute to the enhanced cell proliferation observed in the long-term culture experiments described above.

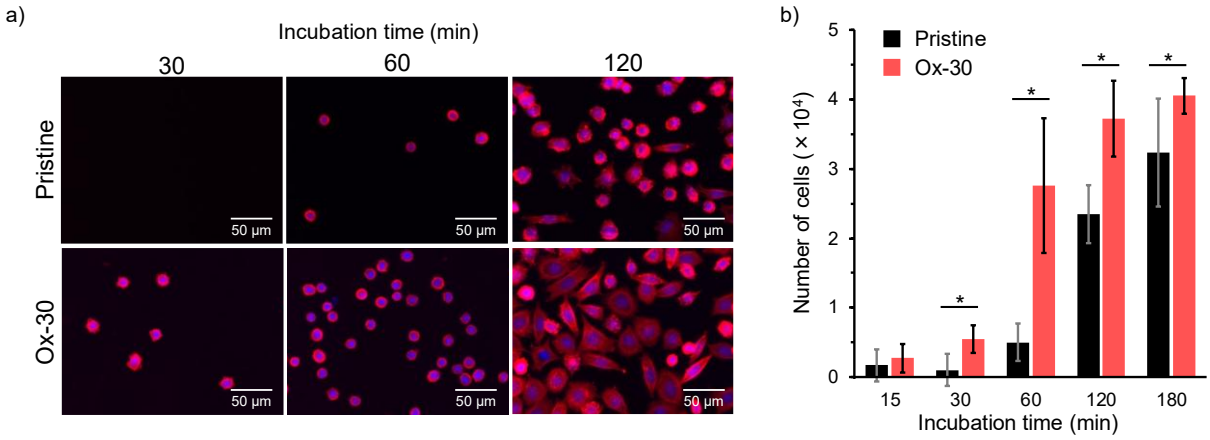

Figure 6. (a) Fluorescence microscopy images of L929 cells stained for actin filaments (red) and nuclei (blue) after incubation for 30–120 minutes. (b) Quantification of adherent cells on PLA films after incubation for 15–180 minutes (n = 4). Statistical significance was determined using the Student's *t*-test. Error bars represent standard deviation. * $p < 0.05$.

To clarify the mechanism underlying the enhancement of cell affinity induced by photo-oxidation, the carboxy groups introduced during photo-oxidation were used as reactive sites for further modification with DA, and the effect on cell affinity was evaluated. This experiment was designed to specifically elucidate the role of photo-oxidation–introduced carboxy groups in modulating cell affinity. For this analysis, L929 cells were seeded at a density of 1×10^4 cells/well on PLA films and cultured for 3 days. Cell counting was then performed, and cell morphology was examined. Cell affinity was evaluated for three sample groups: pristine, Ox-30, and Ox-30-DA. Morphological observations revealed that numerous cells with extended actin filaments were present on Ox-30, whereas cells on Ox-30-DA were predominantly spherical, similar to those on pristine samples (Figure 7a). Quantification of cell numbers demonstrated that Ox-30-DA had a cell count comparable to that of pristine PLA, and both were significantly lower than cell counts

in Ox-30 (Figure 7b). These results indicate that the carboxy groups introduced under moderate oxidation conditions play a critical role in promoting cell adhesion. The decrease in adhesion upon amidation suggests that Ox-30 represents an optimal interfacial state in which carboxyl group density, surface charge, and wettability are balanced to favor cell attachment. Cell affinity was also evaluated for Ox-60 under the same conditions, with cells seeded at 1×10^4 cells/well and cultured for 4 days. In contrast, Ox-60 exhibited markedly reduced cell adhesion despite possessing the highest carboxy density and most negative zeta potential. Importantly, as shown in Table 3, water contact angle measurements indicate that Ox-60 exhibited significantly increased hydrophobicity compared with Ox-30. As discussed in Section 3.1.2 and shown in Figure 3, oxidation at elevated temperature increased surface roughness and altered apparent wettability.

Although Ox-60 exhibited the highest total protein adsorption (Figure 4), this did not translate into enhanced cell adhesion. Cell adhesion on polymeric substrates is mediated by serum protein adsorption. Although the present study quantified total protein adsorption, the biological activity of the adsorbed protein layer depends not only on its quantity but also on its conformation and orientation at the interface. Previous studies have demonstrated that surface charge density, wettability, and microtopography can influence protein structural rearrangement and exposure of integrin-binding domains. It is well established that optimal cell adhesion occurs within an intermediate wettability window (typically contact angles of ~50–70°),[28] while highly hydrophobic surfaces, although promoting greater total protein adsorption, often induce conformational rearrangements that reduce integrin-binding activity. Therefore, the reduced cell adhesion observed for Ox-60 is likely the result of a combined effect of excessive surface charge density, surface chemical heterogeneity, and microstructural roughening, which together alter the bioactivity and presentation of the adsorbed protein layer.

Interestingly, Ox-60-DA restored cell adhesion to a level comparable to that of pristine PLA (Figure 7c,d). This recovery suggests that partial amidation alleviated the excessive negative surface charge and moderated the interfacial physicochemical state, further supporting the concept that an optimal oxidation window governs cell adhesion behavior. These contrasting trends indicate that cell adhesion is not governed solely by the presence of carboxy groups, but by the magnitude of surface charge density and its balance with wettability and topography.

Taken together, these results demonstrate that surface functionalization does not monotonically improve cell affinity; rather, cellular responses emerge from the interplay of chemical functionality, surface charge density, wettability, and topography. Surface charge is known to influence protein adsorption and subsequent cell–material interactions, thereby affecting cell adhesion and spreading.[27, 28] However, cellular responses to charged surfaces can be cell-type dependent due to differences in membrane composition, integrin expression profiles, and adhesion signaling pathways. Therefore, while similar trends may be expected for other adherent cell types, quantitative behavior may vary and warrants further investigation.

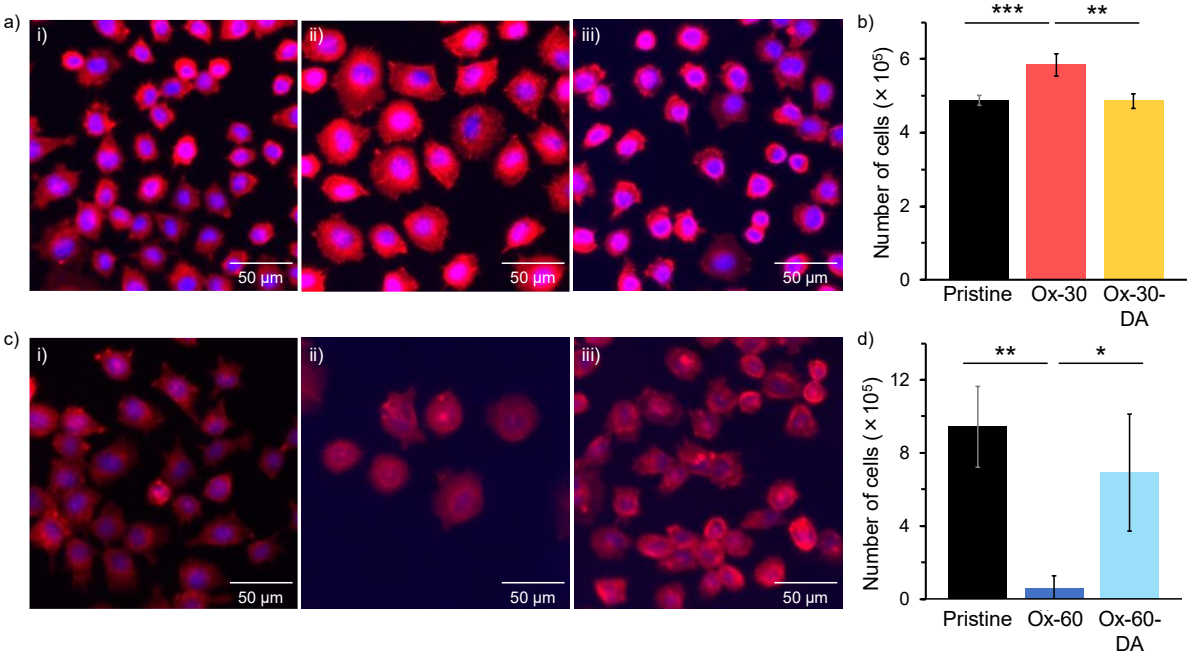

Figure 7. (a) Fluorescence microscopy images of L929 cells stained for actin filaments (red) and nuclei (blue): (i) pristine, (ii) Ox-30, and (iii) Ox-30-DA. (b) Quantification of adherent cells on pristine, Ox-30, and Ox-30-DA PLA films after 3 days of culture (n = 4). Statistical significance was determined using the Student's *t*-test. Error bars represent standard deviation. $^{**}p < 0.01$, $^{***}p < 0.001$. (c) Fluorescence microscopy images of L929 cells stained for actin filaments (red) and nuclei (blue): (i) pristine, (ii) Ox-60, and (iii) Ox-60-DA. (d) Quantification of adherent cells on pristine, Ox-60, and Ox-60-DA PLA films after 4 days of culture (n = 4). Statistical significance was determined using the Student's *t*-test. Error bars represent standard deviation. $^{*}p < 0.05$, $^{**}p < 0.01$.

3.2.3 Stability and Mechanical Integrity Compared with Conventional Treatments

Conventional plasma treatments are widely used to introduce oxygen-containing functionalities onto polymer surfaces; however, such modifications have often been reported to diminish over time under ambient or aqueous conditions. In contrast, the photo-oxidized PLA surfaces prepared in this study exhibited stable surface properties under both aqueous exposure and long-term storage conditions.

To evaluate stability under biologically relevant conditions, oxidized samples were immersed in Milli-Q water or cell culture medium for 3 days under the same conditions used for cell culture. Quantitative analysis of surface carboxy groups by TBO staining yielded values comparable to those obtained prior to immersion (Figure S2), indicating no apparent loss of surface carboxy functionality during aqueous exposure.

Furthermore, oxidized samples stored under ambient conditions were evaluated immediately after treatment and after 3 and 6 months of storage. Cell adhesion assays performed simultaneously

for these samples showed no statistically significant differences in cell affinity among the three groups (Figure S3), demonstrating that the enhanced cell adhesion behavior was maintained for at least six months. These results suggest that the present photo-oxidation approach provides improved long-term stability compared with conventional plasma treatments under the conditions examined in this study.

In addition to surface stability, preservation of bulk mechanical properties is critical for practical applications. Tensile testing was performed on untreated PLA and samples subjected to plasma treatment, photo-oxidation, and alkaline hydrolysis (Figure S4). The untreated PLA exhibited a tensile strength of approximately 60 MPa. Both plasma-treated and photo-oxidized samples showed tensile strengths comparable to the untreated material, with no statistically significant differences. In contrast, alkaline hydrolysis treatment resulted in a marked decrease in tensile strength to approximately 45 MPa.

These results indicate that, whereas alkaline treatment compromises bulk mechanical integrity due to chain scission and hydrolytic degradation, the present photo-oxidation method achieves effective surface functionalization while preserving the intrinsic mechanical properties of PLA. Taken together, the demonstrated long-term surface stability and retention of mechanical strength highlight the practical advantages of the present method over conventional plasma and alkaline surface modification techniques.

3.2.4 Cell culture on 3D structures

To evaluate the cell affinity of photo-oxidized 3D structures, L929 cells were seeded at a density of 1×10^4 cells/well on pristine, Ox-30, and Ox-60 scaffolds and cultured for 3 days (Figure 8a).

Quantification of cell numbers revealed that Ox-30 exhibited a significant increase in adherent cells compared with that on pristine scaffolds (Figure 8c). Furthermore, morphological analysis demonstrated that cells on Ox-30 displayed elongated actin filaments, indicating improved cell spreading and suggesting enhanced cell affinity (Figure 8b). In contrast, Ox-60 showed a significantly lower number of adherent cells than pristine scaffolds. This reduction in cell affinity at 60 °C cannot be explained solely by surface carboxy density or total protein adsorption. Although Ox-60 exhibited the highest total protein adsorption (Figure 4), it showed reduced cell attachment. These results indicate that total protein quantity alone does not determine cellular responses. The high density of carboxy groups introduced at 60 °C renders the surface strongly negatively charged, and this electrostatic environment—together with the increased surface roughness and altered wettability—may influence the adsorption behavior of cell adhesion proteins. It is well recognized that cell adhesion depends not only on the amount of adsorbed protein but also on its conformation, orientation, and bioactivity. Therefore, the reduced cell affinity observed for Ox-60 is more plausibly attributed to qualitative alterations in the adsorbed protein layer arising from the combined effects of surface charge, wettability, and morphology, rather than from carboxy density alone.[28]

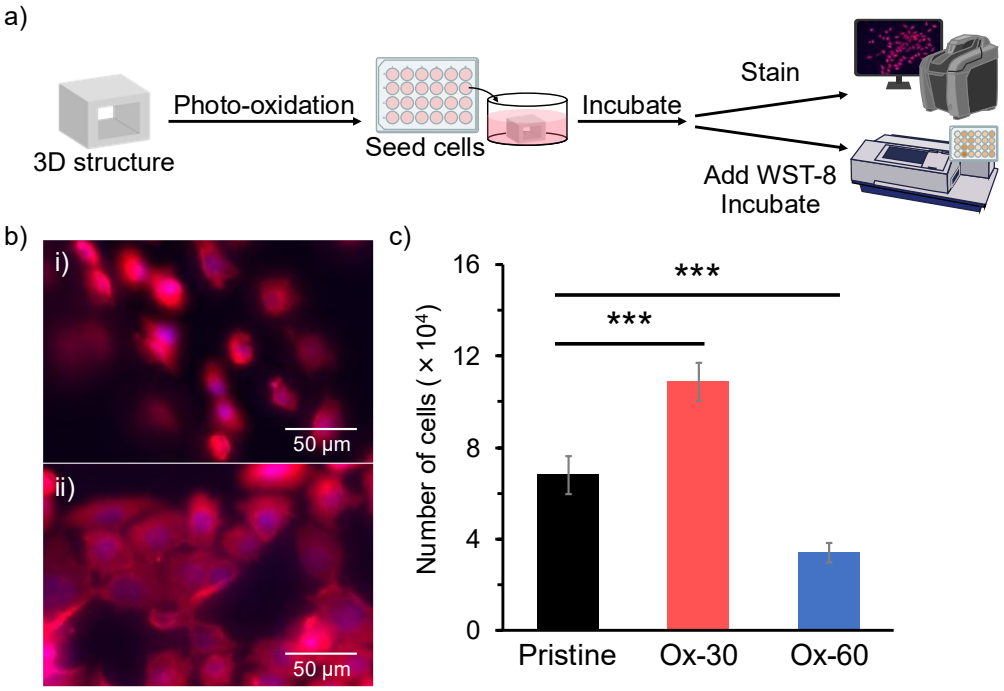

Figure 8. (a) Schematic diagram of the cell culture experiment on 3D-printed PLA scaffolds. (b) Fluorescence microscopy images of L929 cells stained for actin filaments (red) and nuclei (blue): (i) pristine and (ii) Ox-30. (c) Quantification of adherent cells on 3D structures after 3 days of culture (n = 4). Statistical significance was determined using the Student's t-test. Error bars represent standard deviation. *** $p < 0.001$.

In this study, the influence of surface charge and chemical functional groups on cell adhesion behavior was evaluated using L929 fibroblasts. L929 cells are widely used as a standard attachment-dependent model for assessing the cell compatibility of materials and were chosen here to elucidate the fundamental effects of surface modification on cell–material interfacial interactions.

The regulation of cellular responses by surface charge and chemical properties has been extensively reported in the field of materials science. For example, surface potential and charge

can modulate protein adsorption, thereby influencing cell adhesion, proliferation, and differentiation.[29] Moreover, surface functional groups and wettability have been shown to directly affect protein adsorption and cell attachment.[30] These findings support the notion that cell adhesion is a general interfacial phenomenon that depends not only on intrinsic cell properties but also on the surface charge state and interfacial chemistry of the material.

However, membrane composition, glycan structures, integrin expression levels, and differentiation state vary among cell types, potentially affecting the extent and pattern of responses to identical surface chemistries. The surface charge-dependent adhesion observed in this study is considered to result primarily from the influence of surface charge on protein adsorption and initial adhesion, although the magnitude of this effect and subsequent cellular responses may be cell type-dependent.

Therefore, the surface modification strategy proposed herein should be regarded not as an optimization for a specific cell type, but as a design principle enabling modulation of cellular responses through the control of surface charge and chemical functional groups. Future studies involving a variety of cell types, including stem cells and differentiation-specific cells, are required to further clarify the applicability of this approach in biomaterial design and its translational significance.

4. Conclusion

In this study, PLA was photo-oxidized to fabricate scaffolds with enhanced cell affinity. Both film-like and 3D-printed PLA structures were subjected to photo-oxidation. This treatment preferentially introduced carboxy groups onto the PLA surface, thereby improving its hydrophilicity. As a result, cell affinity toward the photo-oxidized PLA increased, an effect attributed to the presence of the introduced carboxy groups. Furthermore, the results demonstrated that this photo-oxidation method is applicable to complex 3D structures.

These findings contribute to the development of a fundamental technology for controlling cell affinity through a surface modification approach for polymer resins. The photo-activated $ClO_2^{\bullet}$-based modification method is broadly applicable to various C–H–containing polymer resins, enabling the introduction of oxygen-containing functional groups. This strategy can be applied not only for the preparation of scaffold materials but also as a platform for further functionalization starting from these introduced functional groups.

5. Author information

Corresponding Author

Haruyasu Asahara

Graduate School of Pharmaceutical Sciences, The University of Osaka, Yamada-oka 1-6, Suita, Osaka, 565-0871, Japan.

Email: asahara@phs.osaka-u.ac.jp

Author Contributions

N.O. and H.A. designed the study; N.O. and Y.Y. performed the experiments and analyzed the data; A.N. and H.A. assisted N.O. and Y.Y. with the experiments and analysis; N.O., A.N. and H.A. wrote the manuscript; A.N., T.T., and H.A. provided technical support and conceptual advice; T.I. supervised the project. All the authors discussed the results and commented on the manuscript. All the authors approved the final version of the manuscript.

Acknowledgments

This work was supported by JST SPRING grant (JPMJSP2138, N.O.), the Japan Society for the Promotion of Science (JSPS) KAKENHI grant (20K05606, H.A.), the New Energy and Industrial Technology Development Organization (NEDO) grants (17101509–0 & 24000999–0, H.A.) the JST OPERA (Open Innovation with Enterprises, Research Institute, and Academia) grant (JPMJOP1861, T.I.), and Research Support Project for Life Science and Drug Discovery (Basis for Supporting Innovative Drug Discovery and Life Science Research (BINDS)) from AMED (JP22ama121054, T.I.).

Data availability

The data supporting the findings of this study are available from the corresponding author upon reasonable request.

6. Supporting information

Comparison of amidation with and without NHS by TBO assay (Figure S1); stability of surface carboxy groups after immersion in Milli-Q water and cell culture medium (Figure S2); cell proliferation after long-term storage (Figure S3); maximum tensile strength of PLA films subjected to different surface modification methods (Figure S4).

7. References

1. Donate, R.; Monzón, M.; Alemán-Domínguez, M. E. Additive Manufacturing of PLA-Based Scaffolds Intended for Bone Regeneration and Strategies to Improve Their Biological Properties. *E-Polym.* **2020**, *20* (1), 571–599. DOI: 10.1515/epoly-2020-0046

2. Castro-Aguirre, E.; Iñiguez-Franco, F.; Samsudin, H.; Fang, X.; Auras, R. Poly(Lactic Acid)—Mass Production, Processing, Industrial Applications, and End of Life. *Adv. Drug Deliv. Rev.* **2016**, *107*, 333–366. DOI: 10.1016/j.addr.2016.03.010

3. Yang, Z.; Yin, G.; Sun, S.; Xu, P. Medical Applications and Prospects of Polylactic Acid Materials. *iScience* **2024**, *27* (12), 111512. DOI: 10.1016/j.isci.2024.111512

4. Bülow, A.; Schäfer, B.; Beier, J. P. Three-Dimensional Bioprinting in Soft Tissue Engineering for Plastic and Reconstructive Surgery. *Bioengineering* **2023**, *10* (10), 1232. DOI: 10.3390/bioengineering10101232

5. Roach, P.; Farrar, D.; Perry, C. C. Interpretation of Protein Adsorption: Surface-Induced Conformational Changes. *J. Am. Chem. Soc.* **2005**, *127* (22), 8168–8173. DOI: 10.1021/ja042898o

6. Jia, L.; Zhang, P.; Ci, Z.; Zhang, W.; Liu, Y.; Jiang, H.; Zhou, G. Immune-Inflammatory Responses of an Acellular Cartilage Matrix Biomimetic Scaffold in a Xenotransplantation

Goat Model for Cartilage Tissue Engineering. *Front. Bioeng. Biotechnol.* **2021**, *9*. DOI: 10.3389/fbioe.2021.667161

7. Srivastava, A.; Bhati, P.; Singh, S.; Agrawal, M.; Kumari, N.; Vashisth, P.; Chauhan, P.; Bhatnagar, N. A Review on Polylactic Acid-Based Blends/Composites and the Role of Compatibilizers in Biomedical Engineering Applications. *Polym. Eng. Sci.* **2024**, *64* (3), 1003–1044. DOI: 10.1002/pen.26626

8. Madhavan Nampoothiri, K.; Nair, N. R.; John, R. P. An Overview of the Recent Developments in Polylactide (PLA) Research. *Bioresour. Technol.* **2010**, *101* (22), 8493–8501. DOI: 10.1016/j.biortech.2010.05.092

9. Sitthisang, S.; Hou, X.; Treetong, A.; Xu, X.; Liu, W.; He, C.; Sae-Ueng, U.; Yodmuang, S. Nanomechanical Mapping of PLA Hydroxyapatite Composite Scaffolds Links Surface Homogeneity to Stem Cell Differentiation. *Sci. Rep.* **2024**, *14* (1), 21097. DOI: 10.1038/s41598-024-72073-z

10. Cai, Q.; Wan, Y.; Bei, J.; Wang, S. Synthesis and Characterization of Biodegradable Polylactide-Grafted Dextran and Its Application as Compatilizer. *Biomaterials* **2003**, *24* (20), 3555–3562. DOI: 10.1016/S0142-9612(03)00199-6

11. Baran, E. H.; Erbil, H. Y. Surface Modification of 3D Printed PLA Objects by Fused Deposition Modeling: A Review. *Colloids Interfaces* **2019**, *3* (2), 43. DOI: 10.3390/colloids3020043

12. Deka, M.; Sinha, N.; Das, R.; Hazarika, N. K.; Das, H.; Daurai, B.; Gogoi, M. A Review on the Surface Modification of Materials for 3D-Printed Diagnostic Devices. *Anal. Methods* **2024**, *16* (4), 485–495. DOI: 10.1039/D3AY01742G

13. Elsawy, M. A.; Kim, K.-H.; Park, J.-W.; Deep, A. Hydrolytic Degradation of Polylactic Acid (PLA) and Its Composites. *Renew. Sustain. Energy Rev.* **2017**, *79*, 1346–1352. DOI: 10.1016/j.rser.2017.05.143

14. Laput, O. A.; Vasenina, I. V.; Shapovalova, Y. G.; Ochered'ko, A. N.; Chernyavskii, A. V.; Kudryashov, S. V.; Kurzina, I. A. Low-Temperature Barrier Discharge Plasma Modification of Scaffolds Based on Polylactic Acid. *ACS Appl. Mater. Interfaces* **2022**, *14* (37), 41742–41750. DOI: 10.1021/acsami.2c11027

15. Nishimura, S.; Hokazono, N.; Taki, Y.; Motoda, H.; Morita, Y.; Yamamoto, K.; Higashi, N.; Koga, T. Photocleavable Peptide–Poly(2-Hydroxyethyl Methacrylate) Hybrid Graft Copolymer via Postpolymerization Modification by Click Chemistry To Modulate the Cell Affinities of 2D and 3D Materials. *ACS Appl. Mater. Interfaces* **2019**, *11* (27), 24577–24587. DOI: 10.1021/acsami.9b06807

16. Ohkubo, K.; Hirose, K. Light-Driven C−H Oxygenation of Methane into Methanol and Formic Acid by Molecular Oxygen Using a Perfluorinated Solvent. *Angew. Chem. Int. Ed.* **2018**, *57* (8), 2126–2129. DOI: 10.1002/anie.201710945

17. Ohkubo, K.; Asahara, H.; Inoue, T. Photochemical C–H Oxygenation of Side-Chain Methyl Groups in Polypropylene with Chlorine Dioxide. *Chem. Commun.* **2019**, *55* (32), 4723–4726. DOI: 10.1039/C9CC01037H

18. Yamamoto, K.; Asahara, H.; Moriguchi, M.; Inoue, T. Immobilization of β-Cyclodextrin onto Polypropylene Nonwoven Fabric Based on Photooxidative Surface Modification. *Polym. J.* **2023**, *55* (5), 599–605. DOI: 10.1038/s41428-022-00751-8

19. Asahara, H.; Wu, W.; Asoh, T.-A.; Hsu, Y.-I.; Inoue, T.; Uyama, H. Surface Modification of Polylactic Acid Using a Photo-Activated Chlorine Dioxide Process: Surface Properties and Dissimilar Adhesion. *Mater. Adv.* **2025**, *6* (5), 1608–1612. DOI: 10.1039/D4MA01275E

20. Jia, Y.; Chen, J.; Asahara, H.; Asoh, T.-A.; Uyama, H. Polymer Surface Oxidation by Light-Activated Chlorine Dioxide Radical for Metal–Plastics Adhesion. *ACS Appl. Polym. Mater.* **2019**, *1* (12), 3452–3458. DOI: 10.1021/acsapm.9b00871

21. Sano, S.; Kato, K.; Ikada, Y. Introduction of Functional Groups onto the Surface of Polyethylene for Protein Immobilization. *Biomaterials* **1993**, *14* (11), 817–822. DOI: 10.1016/0142-9612(93)90003-K

22. Nakayama, Y.; Takahagi, T.; Soeda, F.; Hatada, K.; Nagaoka, S.; Suzuki, J.; Ishitani, A. XPS Analysis of NH3 Plasma-Treated Polystyrene Films Utilizing Gas Phase Chemical Modification. *J. Polym. Sci. Part Polym. Chem.* **1988**, *26* (2), 559–572. DOI: 10.1002/pola.1988.080260219

23. Tamada, Y.; Ikada, Y. Cell Adhesion to Plasma-Treated Polymer Surfaces. *Polymer* **1993**, *34* (10), 2208–2212. DOI: 10.1016/0032-3861(93)90752-V

24. Wang, Y.; Ma, K.; Xin, J. H. Stimuli-Responsive Bioinspired Materials for Controllable Liquid Manipulation: Principles, Fabrication, and Applications. *Adv. Funct. Mater*. **2018**, *28* (6), 1705128. DOI: 10.1002/adfm.201705128

25. Tümer, E. H.; Erbil, H. Y.; Akdoğan, N. Wetting of Superhydrophobic Polylactic Acid Micropillared Patterns. *Langmuir* **2022**, *38* (32), 10052–10064. DOI: 10.1021/acs.langmuir.2c01708

26. Hynes, R. O. Integrins: Bidirectional, Allosteric Signaling Machines. *Cell* **2002**, *110* (6), 673–687. DOI: 10.1016/S0092-8674(02)00971-6

27. Keselowsky, B. G.; Collard, D. M.; García, A. J. Surface Chemistry Modulates Fibronectin Conformation and Directs Integrin Binding and Specificity to Control Cell Adhesion. *J. Biomed. Mater. Res. A* **2003**, *66A* (2), 247–259. DOI: 10.1002/jbm.a.10537

28. Arima, Y.; Iwata, H. Effect of Wettability and Surface Functional Groups on Protein Adsorption and Cell Adhesion Using Well-Defined Mixed Self-Assembled Monolayers. *Biomaterials* **2007**, *28* (20), 3074–3082. DOI: 10.1016/j.biomaterials.2007.03.013

29. Hatakeyama, M.; Kitaoka, T. Surface-Carboxylated Nanocellulose-Based Bioadaptive Scaffolds for Cell Culture. *Cellulose* **2022**, *29* (5), 2869–2883. DOI: 10.1007/s10570-021-04154-5

30. Metwally, S.; Stachewicz, U. Surface Potential and Charges Impact on Cell Responses on Biomaterials Interfaces for Medical Applications. *Mater. Sci. Eng. C* **2019**, *104*, 109883. DOI: 10.1016/j.msec.2019.109883

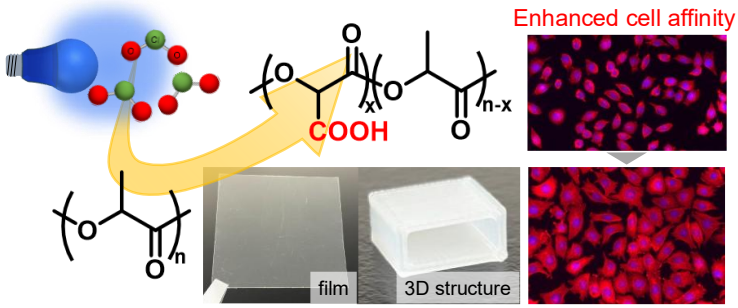

TOC Graphic